



GIS-based fuzzy comprehensive evaluation of urban flooding risk with socioeconomic index system development

Fei Li^{1,2} · Jieru Yan¹ · Xiaolan Xiong¹ · Hexiang Yan¹ · Tao Tao¹ · Linsen Wang¹

Received: 8 November 2022 / Accepted: 12 February 2023 / Published online: 2 March 2023
© The Author(s), under exclusive licence to Springer-Verlag GmbH Germany, part of Springer Nature 2023

Abstract

Due to the climate change-induced extreme rainfall, urban flooding risk is one of the major concerning risks in the near future with accelerating occurrence frequency and intensity. To systematically evaluate the socioeconomic impacts induced by urban flooding, this paper proposed a GIS-based spatial fuzzy comprehensive evaluation (FCE) framework for local government to efficiently take contingency measures especially under urgent rescue conditions. The risk-assessing procedure could be investigated in 4 aspects: 1) application of the hydrodynamic model to simulate the depth and extent of inundation; 2) quantification of the impact of flooding with 6 methodically picked evaluation indexes concerning the transportation attenuation, residential security, and tangible and intangible monetary losses according to depth-damage functions; 3) implementing FCE method: comprehensive evaluation of urban flooding risk with the diverse socioeconomic indexes by fuzzy theory; and 4) presenting the risk maps of single and multiple impact factors intuitively in ArcGIS platform. The detailed case study in SA city validates the effectiveness of the adopted multiple index evaluation framework, which could help detect higher risk areas with low transport efficiency, high economic loss, high social impact, and high intangible damage. The results of single-factor analysis can also provide feasible suggestions for decision-makers and other stakeholders. Theoretically, the proposed method tends to improve the evaluation accuracy as the inundation distribution can be simulated by hydrodynamic model rather than subjective prediction with hazard factors, while the impact quantification with flood-loss models can also directly reflect the vulnerability of involved factors instead of empirical weight analysis of traditional methods. Besides, the results illustrate that the areas with higher risk levels reasonably coincide with severe inundation situations and dense hazard-bearing bodies. This systematic evaluation framework can support applicable references for further extension to other similar cities.

Keywords Urban flooding · Risk assessment · Geographic information system · Multiple index evaluation framework · Flood-loss model

Introduction

According to the Intergovernmental Panel on Climate Change (IPCC) Sixth Assessment Report (IPCC 2022), the impacts of climate change indicate that climate risks

are appearing faster and will get more severe sooner with high confidence. Actually, global risk perceptions highlight societal and environmental concerns, especially for the top short-term risk of extreme weather events (The Global Risks Report 2022). Recently, with the accelerated urbanization process all over the world and the frequent occurrence of extreme rainfall due to the climate change, urban flooding has become a notable threat on the human communities at global and regional levels (Li et al. 2015). In China, flooding risk is perceived to be one of the major concerning risks in the near future with increasingly occurrence frequency and intensity (Zheng et al. 2022). From July 18 to 21, 2021, Zhengzhou in Henan province suffered an extreme precipitation in history (i.e., “Zhengzhou 7.20 Storm”), resulting in devastating flooding disasters with 380 casualties and

Responsible Editor: Philippe Garrigues

Fei Li and Jieru Yan contributed equally to this work.

✉ Hexiang Yan
hxyan@tongji.edu.cn

¹ College of Environmental Science and Engineering, Tongji University, 1239 Siping Road, Shang Hai 200092, People's Republic of China

² Shanghai Huishui Technology Company, Yangpu, Shang Hai 200090, People's Republic of China

RMB 40.9 billion of direct property losses (Xinhua News Agency 2022). Actually, the reported flooding tragedies indicate that current assessment of urban flooding risk and the according contingency scheme for mitigating flooding disasters are far from satisfactory, especially under unexpected weather in most of the central areas of megacities in China with considerable economic and political status. As a consequence, it is of great significance to efficiently evaluate the social and economic impacts of flooding risk to reduce the urban flooding loss.

Flooding risk assessment is synthetically related to several factors including 3 aspects: “hazard,” “exposure,” and “vulnerability.” Specifically, “hazard” relates to disaster-inducing factors commonly exemplified as precipitation, intensity, and frequency of rainfall (discussed in Wang et al. 2011; Lai et al. 2015; Lv et al. 2020); “exposure” stands for hazard-related environment such as ground elevation condition, slope, or impermeability (referred in Lai et al. 2015; Cai et al. 2019); “vulnerability” represents the hazard-bearing body, which is affected by the flooding, usually illustrated as building, transportation, population, and economic indexes (analyzed in Geng et al. 2020; Lv et al. 2020). Sometimes, the hazard-related “exposure” is also regarded as “hazard,” so the risk is the product of “hazard” and “vulnerability” (Geng et al. 2020). Concerning these intricate factors entangled in the risk assessment process, Zheng et al. (2022) suggested that the application of fuzzy theory is favorable to deal with the multiple-index evaluation system for efficiently reducing the involved uncertainty of estimation issues. Fuzzy comprehensive evaluation (FCE), one of the fuzzy mathematics methods, is considered as a more qualified method for ranking multiple hazard factors and mapping the comprehensive risk level distribution with various vulnerability indexes (Lai et al. 2015; Geng et al. 2020). With the development of more advanced hydrodynamic models, numerical simulations can provide more accurate estimations of the submerged area, inundation depth, as well as flooding duration rather than roughly estimated by some related indicators such as precipitation, drainage network condition, or impermeable index (Teng et al. 2017; Cai et al. 2019; Geng et al. 2020; Brussee et al. 2021). Ideally, the numerical hydraulic simulation results should be well incorporated with relevant topographic, social, or economic characteristics in a unified platform. Practically, the potent geostatistical tool in ArcGIS platform can provide digital backing and applicative support for multidimensional risk assessment (Gigovic et al. 2017), which can well integrate the flooding information simulated by stormwater models such as InfoWorks Integrated Catchment Modeling (ICM) (Wallingford 1981) program with the local characteristics, so as to establish a systematic

evaluation framework for the final synthesis risk evaluation with the integrated GIS techniques in an intuitively visualized platform in this work.

In contrast, loss estimation and evaluation of disaster consequences are also indispensable parts of flood risk assessment (Win et al. 2018), and the results can support better risk reduction strategies for decision-makers with more targeted tool of flood-loss models to specify the “hazard”—“vulnerability” relationship. Straightforwardly, depth of water is often considered as the only hazard factor affecting the damage in most studies (Marvi2020), and the derived models usually describe the relationship between flood depth and the damage extent (commonly expressed by monetary quantity) of specific objects such as buildings and indoor assets. Many researchers applied the effective method to assess the flood damage; for instance, Win et al. (2018) derived flood damage function models to evaluate the house damage, in-house damage, and income loss in the studied residential and agricultural areas in the Bago River basin, Myanmar; Oubennaceur et al. (2019) estimated the expected annual damage of each individual building with the derived depth-vulnerability relationship in the study area in Quebec, Canada and presented a local scale risk map for better risk decision-making. Wang et al. (2021) successfully achieved the goals of identifying a significant area in Beijing with high-risk level and evaluating the economic loss of buildings in the identified area by deriving depth-damage functions. Compared to the hazard-exposure-vulnerability index-based system assessed by fuzzy methods, most of the risk-related factors have been integrated to the depth-damage functions with highly simplified parameters. However, the transferability of the models is suspicious as socioeconomic characteristics may vary spatially and temporally for different studied areas (Gerl et al. 2016). As reviewed by Marvi (2020), the empirical models using real data could be exclusively applied to targeted region with similar damage types and flood characteristics, while developing analytical models using what-if analysis are very expensive and time-consuming with better flexibility. Generally, only one or two critical damage types would be discussed in detail for the studied areas due to the laborious process for establishing and validating the flood-loss models. In this work, more representative types of flooding damage would be analyzed.

For the involved risk-rating index system, previous bodies of literature indicate that the risk index selection process may vary from areas to areas based on different local characteristics (Tehrany et al. 2013), as one high-impact index may turn out to be negligible in another area (Kia et al. 2012). Based on the accessibility of flood-loss models which can be easily adopted in similar cities in

China and the available database from local government, the scrupulously selected socioeconomic impact indexes in this study would consist of the road traffic velocity attenuation, building structure damage, property losses, residential security, public psychology, and influences on production efficiency. Specifically, quantification of direct damage (including building structure damage and property losses) plays a pivotal role in flood risk assessment for various stakeholders especially for insurance in developed countries, and it is most commonly studied (Marvi 2020; Nithila et al. 2022). For the indirect impacts which are difficult to express in monetary terms, transportation impacts are often ignored despite its significance to ensure daily operation of a city (Hammond et al. 2015). Dutta et al. (2003) noticed that the time costs were significantly greater than the marginal expenses of traffic, so the attenuation of road traffic velocity would be further examined instead of estimating the cost of traffic disruption in this work. Besides, the intangible damage, which principally consists of physical and mental health effects, has contributed consequential social impacts to evaluate the comprehensive flood losses (Hudson et al. 2019; Dassanayake et al. 2015). Accordingly, three main categories of intangible losses were considered in this study: residential casualties, public psychology, and influences on production efficiency. Based on the estimation results, the government can implement necessary strategies for rescue operation and the involved individuals can effectively cultivate the risk awareness to protect themselves. According to the investigation panel of “Zhengzhou 7.20 Storm,” which comprised the experts in Ministry of Water Conservancy, Ministry of Transport, Ministry of Housing and Urban–Rural Development, National Development and Reform Commission and Commission on Health (Xinhua News Agency 2022), most of the involved socioeconomic parameters are accessible from these rescue departments.

Despite the previous researchers having accomplished considerable progresses in this field of urban flooding risk assessment, there still exist several shortcomings and deficiencies. Actually, FCE method is preponderant to roughly assess the flood risk distribution and identify the most critical factor among the involved risk-rating index system even with inadequate monitoring data (Geng et al. 2020), while flood-loss models tend to provide highly effective approach of particular risk-reduce objectives based on empirical damage data from specific case studies. Apparently, the case studies in Shanghai (Quan 2014a, b), Beijing (Wang et al. 2021), and Shenzhen (Lyu et al. 2020) could be further improved if more necessary abovementioned objectives could be incorporated in an integrated assessment framework. With the combination of the merits of FCE method and flood-loss models for

the presented multiple-index evaluation framework, this paper aims to propose a feasible procedure for multiple risk assessment which can effectively propose contingency plans for risk reduction in most of the cities in China especially characterized with functional drainage system to support hydraulic simulation, high density of buildings and population, and comparative socioeconomic status under extreme rainstorm conditions.

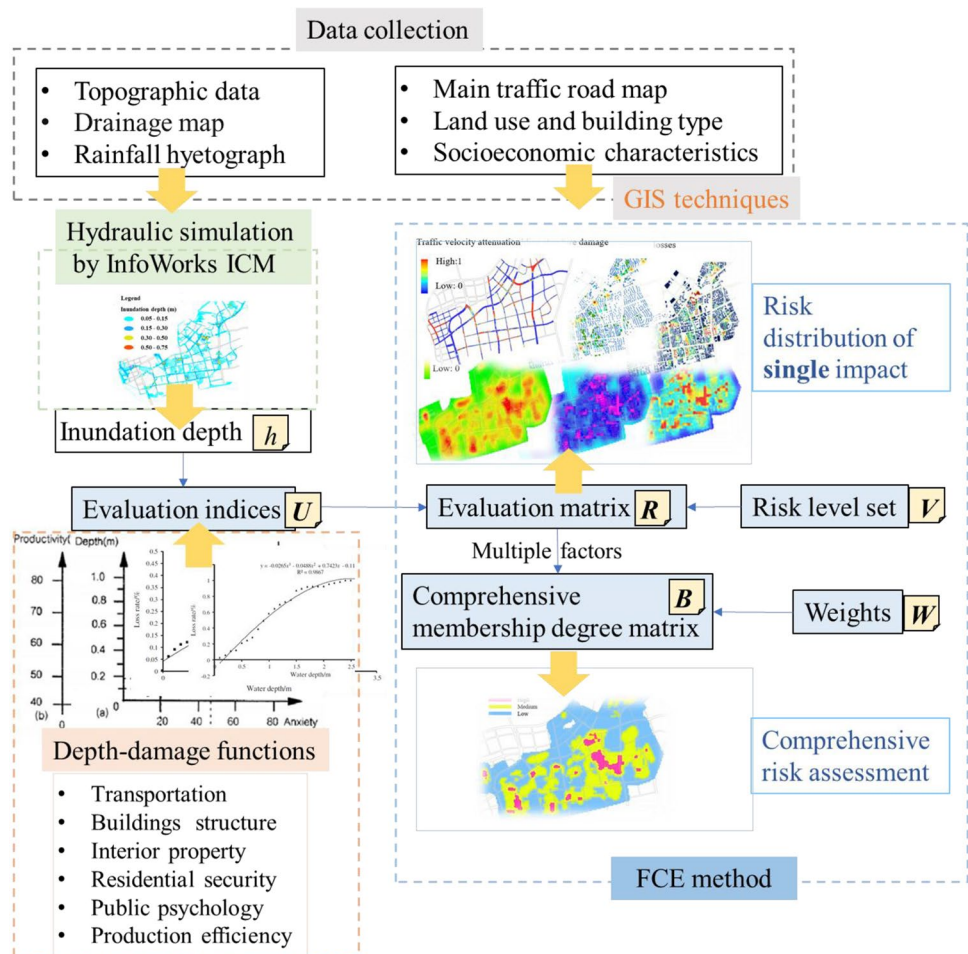
To address the issue of urban flooding risk assessment, this current work has established an integrated systematic assessment framework for multiple objectives to improve the accuracy and efficiency. In the present study, the advanced FCE method was adopted to evaluate the flooding risks with the GIS-based flood-loss model to quantify 6 socioeconomic indexes in the second section, followed by a case study in real-life area in SA city in the third section, demonstrating the flooding risk assessment results. Finally, the fourth and the fifth sections summarize the results and conclusions, respectively.

Methodology

Conceptual framework of GIS-based flooding risk assessment

The flow diagram of the proposed GIS-based flooding risk assessment process is summarized in Fig. 1. First, for the data collection process, the topography information (such as the land use patterns and district elevation distribution), layout of drainage systems, rainfall hyetograph, building footprints, road layouts, local socioeconomic characteristics, historical or field measured inundation depth, and damage data should be well prepared for model establishment and validation. Accordingly, the inundation distribution could be simulated by InfoWorks ICM program. Based on the depth of inundation, 6 typical types of flood loss would be estimated by the depth-damage functions, and the calculation results are also considered as the selected risk evaluation factors in the index-based system. Afterward, the single-impact evaluation and comprehensive risk assessment of multiple indexes can be conducted by FCE method. Specifically, for the single factor evaluation, the flooding risk is simply estimated by the evaluation matrix R calculated by the membership function of each selected risk factor from the evaluation index U and its ranking index in remarking set V . For more complex situations with multiple impact factors, the final risk of FCE is determined by the comprehensive membership degree matrix B , which is obtained by the fuzzy relation synthetic operation with according evaluation matrix R and weight distribution W . Finally, the evaluation results would be presented in the risk maps of single- and multiple-impact factors intuitively in ArcGIS platform with the integrated visual tools.

Fig. 1 Flowchart of proposed FCE method



Fuzzy comprehensive evaluation (FCE) method

As previously stated, attributed to the superiority of comprehensiveness, accuracy, and intuitiveness, FCE method (Yager 1977; Wang 1983, 2002) is favorable for flooding risk analysis. In the assessment process, the most important part of this method is the establishment of membership functions, which is the core and the difficult part of the assessment. The more extensive and elaborate the membership functions, the more robust and accurate the assessment would be. The selection of risk evaluation factors may vary from area to area due to different local characteristics in each specific flooding district (Kia et al. 2012; Tehrani et al. 2013). In the current study, tangible and intangible criteria of six impact factors including the transportation, building structure, interior property, residential security, public psychology, and production efficiency were considered according to the actual social or economic flooding-inducing conditions and previous bodies of literature (Lai et al. 2015; Geng et al. 2020). As listed in Table 1, the collection of these factors can be expressed by a vector as follows: $U = \{u_1, u_2, u_3, u_4, u_5, u_6\}$,

Table 1 Evaluation factor set and the according critical point of each risk level

Impact factor set	Evaluation indexes	Low risk (v_1)	Medium risk (v_2)	High risk (v_3)
u_1	Transportation	p_{11}	p_{12}	p_{13}
u_2	Building structure	p_{21}	p_{22}	p_{23}
u_3	Interior property	p_{31}	p_{32}	p_{33}
u_4	Residential security	p_{41}	p_{42}	p_{43}
u_5	Public psychology	p_{51}	p_{52}	p_{53}
u_6	Production efficiency	p_{61}	p_{62}	p_{63}

while each factor was divided into three risk levels and the collection can be expressed as $V = \{v_1, v_2, v_3\}$, namely, “low,” “medium,” and “high” levels.

Totally, 6 impact factors of the assessment model will generate $6 \times 3 = 18$ subordinate layers. For the involved critical point (i.e., $p_{i1}, p_{i2}, p_{i3}, i = 1, 2, \dots, 6$) of each risk level, these values can be obtained from ArcGIS by the method of natural

breaks (Jenks) automatically, as the studied data would be classified with geometric interval in “classification” window.

To evaluate the different factors in a unified grading system with varied range and dimension, the membership function can be expressed by the linear interpolation method (Lai et al. 2015) in details as follows:

$$r_{i1} = \begin{cases} 1 & x \leq p_{i1} \\ \frac{p_{i2}-x}{p_{i2}-p_{i1}} & p_{i1} < x < p_{i2} \\ 0 & x \geq p_{i2} \end{cases} \quad (1)$$

$$r_{i2} = \begin{cases} 0 & x \leq p_{i1} \text{ or } x \geq p_{i3} \\ \frac{(x-p_{i1})}{(p_{i2}-p_{i1})} & p_{i1} < x < p_{i2} \\ \frac{(p_{i3}-x)}{(p_{i3}-p_{i2})} & p_{i2} < x < p_{i3} \end{cases} \quad (2)$$

$$r_{i3} = \begin{cases} 0 & x < p_{i2} \\ \frac{(x-p_{i2})}{(p_{i3}-p_{i2})} & p_{i2} < x < p_{i3} \\ 1 & x \geq p_{i3} \end{cases} \quad (3)$$

where x is the attribute value of each factor calculated by corresponding formula and r_{i1} , r_{i2} , and r_{i3} represent the subordination degrees of these factors corresponding to each risk level while i is the index of the factors. p_{i1} , p_{i2} , and p_{i3} are values obtained from ArcGIS by geometric interval method to classify risk levels as mentioned before.

In the present study, fuzzy comprehensive evaluation method is built based on ArcGIS. A single grid in ArcGIS is treated as a basic research unit. According to the actual value of each factor in each grid and membership functions (1)–(3), we can get an evaluation matrix R (shown in formula (4)) of each grid. Membership matrix R can be used for single-factor evaluation of urban flooding.

$$R = \begin{bmatrix} r_{11} & r_{12} & r_{13} \\ r_{21} & r_{22} & r_{23} \\ r_{31} & r_{32} & r_{33} \\ r_{41} & r_{42} & r_{43} \\ r_{51} & r_{52} & r_{53} \\ r_{61} & r_{62} & r_{63} \end{bmatrix} \quad (4)$$

For more complicated multiple-impact-factors evaluation, the weight distribution matrix $W=(W_1 W_2 W_3 W_4 W_5 W_6)$ could be constructed by analytic hierarchy process (AHP) based on expert experience method to determine the relative importance regarding each factor. AHP is one of the most widely adopted approaches to flexibly integrate various assessment factors with impartial and logical classification system (Lyu et al. 2020).

After the membership matrix R and index weight vector W were obtained, the comprehensive evaluation result of

composite degree B can be determined by R and W with the fuzzy relation synthetic operation as follows:

$$B = W \times R = \begin{bmatrix} W_1 & W_2 & W_3 & W_4 & W_5 & W_6 \end{bmatrix} \cdot \begin{bmatrix} r_{11} & r_{12} & r_{13} \\ r_{21} & r_{22} & r_{23} \\ r_{31} & r_{32} & r_{33} \\ r_{41} & r_{42} & r_{43} \\ r_{51} & r_{52} & r_{53} \\ r_{61} & r_{62} & r_{63} \end{bmatrix} = \begin{bmatrix} b_1 & b_2 & b_3 \end{bmatrix} \quad (5)$$

Composite matrix B indicates the membership degree of the grid to each risk level. The risk level of the grid is finally determined by the principle of maximum membership degree (Xue and Yang 2014), which implies that the maximum comprehensive membership degree would be selected as the representative value of risk level. For instance, if the membership values of one grid are $[b_1 b_2 b_3] = [0.355, 0.587, 0.058]$ corresponding to “low,” “medium,” and “high” risk levels, the final risk level of the grid is “medium” risk, determined by the maximum membership degree 0.587 representing the risk level of “medium”.

GIS-based flooding risk assessment factors estimated by depth-damage functions

As previously mentioned, flooding risk assessment would be carried out by 6 different impact factors in evaluation factor set U , which depend on the distribution of the inundation simulated by the InfoWorks ICM model. The corresponding simulation results could be transferred into the comparable “*.shp” file format in ArcGIS platform so as to be further inspected for assessment of each regarding factor. In the assessment process, the “Model builder” mode in the ArcGIS platform could help furnish with a visual programming environment for creating, editing, and managing spatial analysis models, so that the risk of single impact factor could be visually estimated based on the geographic tool set and the corresponding losses database. With multi-impact factor estimation, ArcGIS platform also provides varieties of set theory methods and operator to merge data, including Fuzzy Overlay, Fuzzy And, Fuzzy Or, Fuzzy Product, Fuzzy Sum and Fuzzy Gamma, and so on, so that the fuzzy relation synthetic operation ($W \times R$) could be conveniently enumerated.

Traffic velocity attenuation

The flooding impact on transportation would be assessed by the velocity attenuation of vehicles. As proposed by Zhao (2015), the relationship between vehicle’s velocity decays and inundation depth could be expressed in a hyperbolic tangent function:

$$v = \frac{v_0}{2} \tan h\left(\frac{-h+a}{b}\right) + \frac{v_0}{2} = \frac{v_0}{2} \times \frac{e^{\left(\frac{-h+a}{b}\right)} - e^{-\left(\frac{-h+a}{b}\right)}}{e^{\left(\frac{-h+a}{b}\right)} + e^{-\left(\frac{-h+a}{b}\right)}} + \frac{v_0}{2} \quad (6)$$

where v represents the vehicle's velocity (km/h); v_0 is the reference velocity of local highway (km/h), which is different from each other among different type of highway or road; h is the inundation depth (m); a is the median value of the critical depth of vehicle stagnation; b is attenuation coefficient, and it represents the rate at which the vehicle velocity decreases with the depth, generally varying from 3 to 5, with smaller values indicating faster decay rate.

According to the recent research of actual urban flooding disasters in many large- and medium-scale cities in China (Zhao 2015), the parameter $a = 15$ cm and $b = 3$ were adopted in this study. Besides, we defined $(1 - \frac{v}{v_0})$ as transportation attenuation factor (T) and the new formula would be

$$T = 1 - \frac{v}{v_0} = 1 - \frac{1}{2} \times \left(\frac{e^{\left(\frac{-h+a}{b}\right)} - e^{-\left(\frac{-h+a}{b}\right)}}{e^{\left(\frac{-h+a}{b}\right)} + e^{-\left(\frac{-h+a}{b}\right)}} + 1 \right) = \frac{e^{-\left(\frac{-h+a}{b}\right)}}{e^{\left(\frac{-h+a}{b}\right)} + e^{-\left(\frac{-h+a}{b}\right)}} \quad (7)$$

Building structure damage

To describe the relationship between the building structure damage and flooding impact, it is assumed that the building damage loss can be described by the representative feature of flooding event, such as inundation depth. Note that other impact factors relevant to the building damage, such as the construction materials, may also be considered in the future work, and the following estimation method is just an easy-extended illustration for other potential applications in the limited emergency rescue process with insufficient available data. Besides, as suggested by Zabret et al. (2018), the application of empirical flood-loss models has given better results for one geographical region with similar building and flood event characteristics than for different regions and floods with more diverse properties. Accordingly, the applied depth-damage function (Quan 2014b) was based on the data collected from field surveys in Shanghai, and the location is just adjacent to the studied region.

As presented by Quan (2014b), the relationship between building structural damage and inundation depth can be described by the hazard-affected body vulnerability curve as follows:

$$BSL = 0.006h^3 - 0.032h^2 + 0.169h + 0.041 \quad (8)$$

where BSL is the rate of building structural losses.

Interior property losses

As suggested by Handmer et al. (2002), the interior property loss (I) in different types of houses tends to be consistent when suffering from flooding. Specifically, this assessing factor index would be valued by the indoor property vulnerability curves developed by Quan (2014a), which is calculated by the sum of residential indoor property vulnerability curve (I_1) and other indoor property vulnerability curve (I_2). The detailed estimation formula is shown as follows:

Residential indoor property vulnerability curve is

$$I_1 = -0.026h^3 - 0.049h^2 + 0.742h - 0.115 \quad (9)$$

For other industrial, commercial or public buildings, the indoor storage property vulnerability curve is

$$I_2 = -0.152h^3 - 0.82h^2 + 1.479h - 0.009 \quad (10)$$

Residential casualties

According to the statistics of historical flooding disasters, some researchers indicated that the types of disasters and the locations where flooding disasters occurred are the important factors that lead to population casualties (Jonkman 2005). On the characteristics of urban flooding disaster, inundation depth is considered as one of the most representative features (Herath et al. 2003) as inundated area increases with water level rising, resulting in less refuge areas and higher risk for residents living in low-lying areas.

A vulnerability curve of population casualties is identified by Boyd et al. (2005), and it was adopted in the present study to estimate the risk of residential mortality:

$$RC = \frac{0.34}{1 + e^{20.37 - 6.18h}} \quad (11)$$

where RC indicates residential mortality rate.

Public psychology and its influence on production efficiency

For the intangible flood damage quantification, the following functions concerning public psychological anxiety caused by flooding and its influence on production efficiency defined by Lekuthai and Vongvisessomjai (2001) are

$$Anxiety = f(Flooddepth, Landuse) \quad (12)$$

$$Productivity = f(Anxiety, Income) \quad (13)$$

As stated by Lekuthai and Vongvisessomjai (2001), the public psychological anxiety degree A could be expressed by a function of the inundated water depth as follows:

$$\begin{cases} A = 20 & h = 0(m) \\ A = \frac{\ln(20h)}{0.0362} & 0 < h < 0.9(m) \\ A = 80 & h > 0.9(m) \end{cases} \quad (14)$$

In contrast, the percentage of productivity decline P_r could then be figured out by the psychological anxiety index A :

$$\begin{aligned} P_r = & 100 - (7 \times 10^{-6} \cdot A^4 - 0.0019 \cdot A^3 + 0.178 \cdot A^2 \\ & - 7.5624 \cdot A + 173.84) \end{aligned} \quad (15)$$

$(20 \leq A \leq 80)$

where P_r is the percentage of productivity decline and A is the psychological anxiety factor.

Note that all the empirical and analytical flood-loss models applied for flood damage analysis should be carefully validated according to the local condition. The involved parameters in different flood-loss functions have been fitted based on comparison with observed loss data collected in field surveys.

Case study and analysis

Study area description

The case study in SA city, China is performed for the validation and discussion of the proposed models and methods. The raw data source utilized in this research includes: 1) topography data was originally measured by the Ziyuan3 satellite with a spatial resolution of 25 m (<https://sss.shanghai-map.net/#/>), 2) contour of elevation distribution and related socioeconomic index were supported by the local government, and 3) the rainstorm drainage map and precipitation data were collected from the local Water Group Co., Ltd. Figure 2(a) shows the satellite overview of investigated district and Fig. 2(b) is the elevation distribution map of the study area. The real-life stormwater drainage system (Fig. 2(c))

consists of 192 sub-catchments, 137 main conduits (with pipe diameters ≥ 400 mm and the total length of about 43.5 km), 3 stormwater pump stations, and 3 outfalls, covering the service area of more than 1000 ha.

Modeling of the flooding event

The drainage simulation model for this real-life network had been trained and calibrated for hydrological and hydraulic simulations under specific rainfall condition, in which the “dynamic wave” method and the Hazen–Williams head loss formula were adopted for simulating the stormwater drainage network behaviors. For analysis, the reporting time and routing time were set as 15 s and the duration of typical rainfall in this city was chosen to be 2 h. The duration of the stormwater event in this studied district was set to 8 h in order to simulate the entire process of the water accumulation and recession. In this study, a 50-year return period rainfall event was set for this studied district according to the Standard for Design of Outdoor Wastewater Engineering (SDOWE 2021). The rainfall intensity distribution is shown in Fig. 3. The hydrological process over the catchments was modeled with 2D surface model coupling with the hydraulic process in the pipelines 1D hydraulic model by the calculation code of InfoWorks ICM (model establishment and calibration procedure can refer to Gong et al. 2018 and Wallingford 2015). The established model was validated with some field surveyed pictures and historic water level monitoring data in corresponding area, and detailed run-off process was similar with the situation described in Li et al. (2015). Figure 4 illustrates the submerged area distribution over the studied district, which shows that the majority of the submergence depth of the whole area is under 0.15 m, but it is still worth noting that the inundation depth in minority district has exceeded 0.5 m. The simulation results with inundation depth were then exported to the ArcGIS platform for further flooding risk assessment.

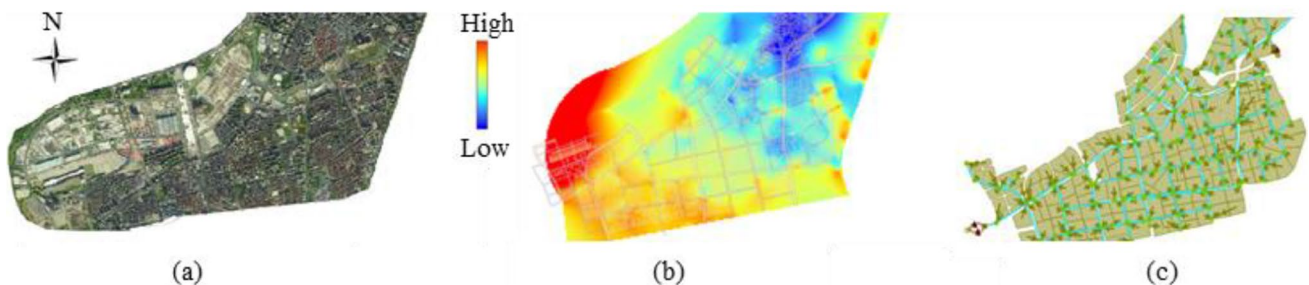


Fig. 2 **a** Satellite overview of research district, **b** contour of elevation distribution of research district, and **c** layout of the sub-catchments of research district in SA city

Fig. 3 Hyetograph of 50-year return period rainfall

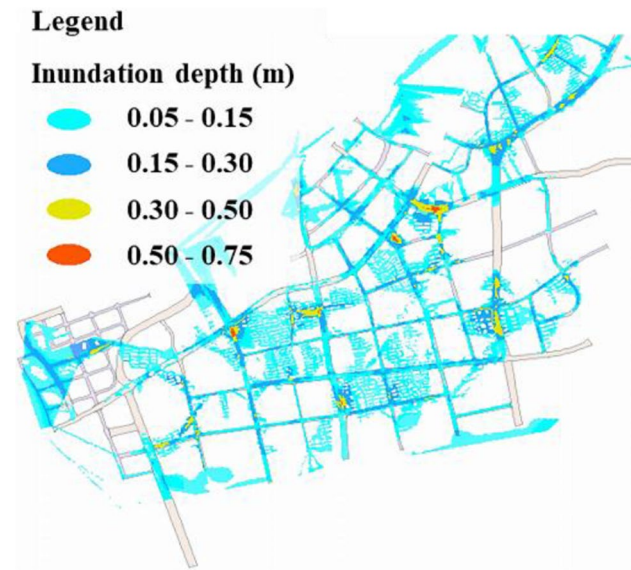
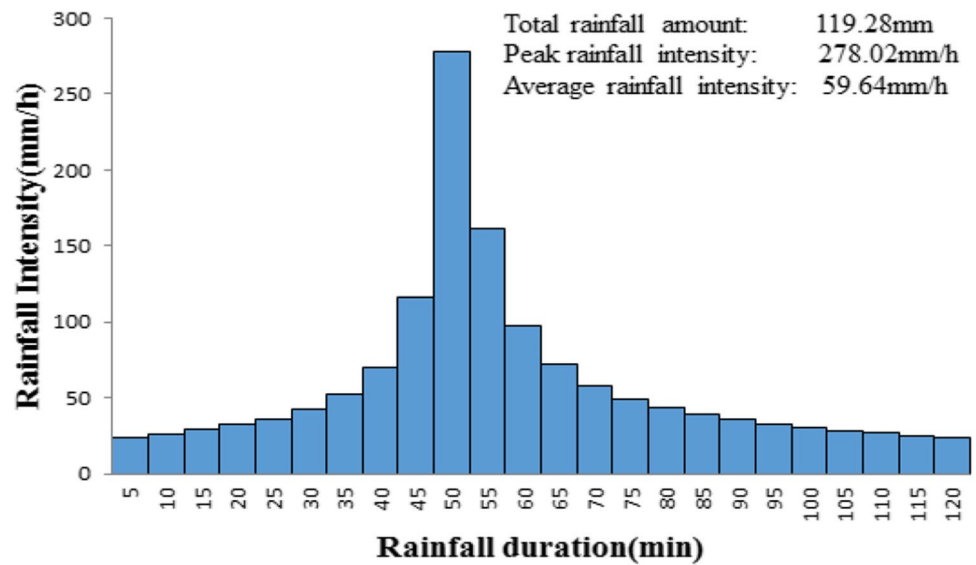


Fig. 4 Distribution of the inundation condition in the studied drainage system in SA city

Results and discussion

Single factor assessment

In the present study, traffic velocity attenuation, building structure damage, interior property losses, residential causalities, public psychology, and production efficiency decline were chosen to be assessment factors. The studied district was divided into many small raster grids with the size of 25 m × 25 m. For each grid, six grid data layers were created, with each grid data layer in ArcGIS

corresponding to one assessment impact factor. Based on the flooding process results obtained in the InfoWorks ICM model, the distribution of the inundation depth could be applied for the evaluation of each flooding risk assessment factor by formulas (7)–(14). Afterward, the grading standard values ($p_{i1}, p_{i2}, p_{i3}, i = 1, 2, \dots, 6$) to discriminate different assessment levels were obtained by geometric interval method in ArcGIS and the results were listed in matrix P .

$$P = [p_{i1}, p_{i2}, p_{i3}] = \begin{bmatrix} 0.35 & 0.72 & 1.00 \\ 0.05 & 0.07 & 0.16 \\ 0.01 & 0.03 & 0.12 \\ 0.0002 & 0.0005 & 0.0021 \\ 1.02 & 2.98 & 11.60 \\ 1.01 & 3.21 & 12.50 \end{bmatrix} \quad (16)$$

where the subscript i represents the selected factors listed in Table 1.

Subsequently, the evaluation matrix R can be established by Eqs. (1)–(3) for single-factor assessment with the critical reference values in matrix P . Consequently, three evaluating layers (high, medium, and low levels of risk) of membership degree can be obtained by the raster calculator function in GIS, and Fig. 5 demonstrates the direct visual map of the assessment result of each single impact factor.

Traffic velocity attenuation

Most of the roads in the studied district were inundated in different extent under a 50-year return period rainfall event scenario. As shown in Fig. 5(a), the red section area indicates that traffic velocity was severely attenuated,

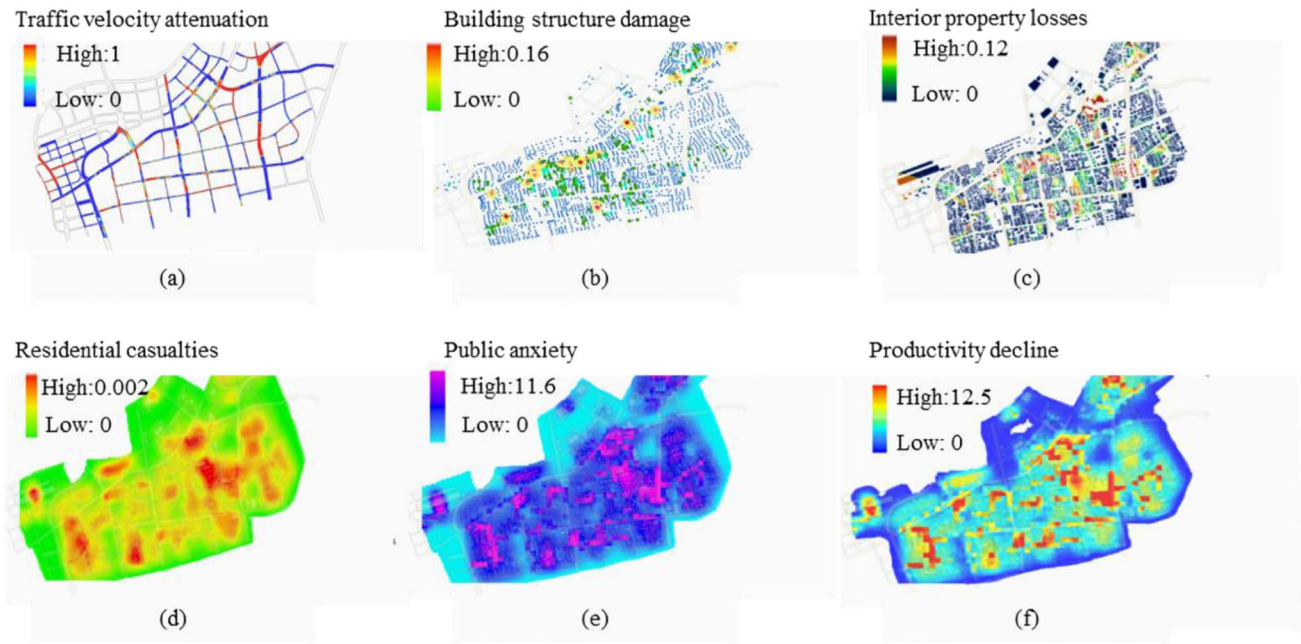


Fig. 5 Spatial distribution of risk assessment based on 6 selected impact factors: **a** traffic velocity attenuation, **b** building structure damage, **c** interior property losses, **d** residential casualties, **e** public anxiety, and **f** productivity decline

which is highly correlated with the inundation zone of the flooding simulation result in Fig. 4. In particular, road traffic was severely interrupted if the inundation depth is more than 30 cm, which means that the transportation attenuation coefficient is approaching 1. This mapping result can significantly provide feasible route planning for more efficient delivery of assistance.

Building structure damage

There are 3728 buildings in the study area and part of buildings suffered from the submerging impact, which leads to structural damage when a 50-year rainfall event is encountered. As shown in Fig. 5(b), 73 buildings are afflicted building structural losses with the rate of more than 0.051 (painted with red color), so corresponding measures should be taken to protect the building structure with this instructive map. As this index of building structural damage follows the exponential function of inundation depth in Eq. (8), the damage could be straightforwardly evaluated and presented with GIS techniques.

Interior property losses

Interior property losses were evaluated based on each building and extracted flooding hazard factors by ArcGIS platform. According to the simulation results, more than 400 buildings were inundated and the maximum water

depth reaches 0.61 m indoor. Detailed distribution of the indoor property losses is shown in Fig. 5(c). Comparing this distribution result with Fig. 2(b), it denotes that areas in lower terrain are easier to encounter intense interior property losses than high-elevation area in the north direction. Besides, the blocks with high building density in southern district also suffer more serious interior property losses. Consequently, this flooding-impact factor is influenced by the topography and site coverage ratio. Moreover, the result indicates that the GIS platform can well integrate the different vulnerability factors of building types with residential, industrial, commercial, or public buildings.

Residential security

The population of the studied district is 5.20 million. Considering the distribution of the population being mainly concentrated on the interior or around buildings, the kernel density analysis was implemented to analyze population spatial distribution density and the closer to buildings, the higher population density is. To modify the range of inundated area by focus statistical tools, the risk factors of spatial population can be calculated by the raster calculator and then multiply with population density grid to get regional residential casualty assessment map (in Fig. 5(d)). Similarly, the result of residential casualty distribution is also highly related to the topography and population density,

so the high-risk casualty area tends to identify the blocks with lower terrain and higher population density.

Public psychology and its influence on production efficiency

On the basis of evaluation method stated previously with formulas (12)–(15), the final psychological anxiety risk values are the product of the population and the psychological anxiety factor A , while production efficiency influence risk values are the product of population and the percentage of productivity decline. The assessment results are shown in Fig. 5(e) and (f), which indicate that the more severe inundation makes more people nervous and anxious. According to historical flooding event record, traffic was interrupted and buildings were inundated or even resulting in resident casualties when the extreme rainfall happens, accompanied by the naturally affected public sentiment as well as the production efficiency. As the factor of production efficiency depends on the variation of psychological anxiety, the distribution pattern of these two factors are quite similar with each other. Consequently, it can be moderately deduced that indexes with the same appraisal object and similar quantitative evaluation approach may lead to resembling classification of risk levels.

Comprehensive risk assessment

As stated previously, the comprehensive risk assessment was estimated by the fuzzy comprehensive analysis. The FCE assessment was finally calculated by 6 impact factors and its weight coefficient. Therefore, before implementation of the comprehensive assessment, it is essential to ascertain an appropriate weight of each factor. In the present study, the weight coefficients were obtained by AHP based on expert

experience, and 10 experts in related field were engaged in the crucial judgment. The final weight vector can be expressed as

$$W = [W_1, W_2, W_3, W_4, W_5, W_6] = [0.36, 0.15, 0.27, 0.10, 0.06, 0.06] \quad (17)$$

where W_1 , W_2 , W_3 , W_4 , W_5 , and W_6 represent the weight coefficient of traffic velocity attenuation, building structure damage, interior property losses, residential casualties, public psychology, and production efficiency, respectively.

It should be noticed that the weight of AHP assumes the traffic velocity attenuation and interior property losses as the top two important indexes among the total 6 factors, which seems reasonable as unimpeded traffic flow signifies better supplementary resource to relieve negative effects of other factors; while most of the inundation depth in the investigated area is under 0.5 m, which appears to be more dangerous for interior property than other concerning factors. Although expert experience as well as many biases due to various opinions may generally affect the intentions to determine the AHP weight, the proposed procedure of GIS-based assessing factors in the “GIS-based flooding risk assessment factors estimated by depth-damage functions” section can furnish better synthetical evaluation performance with less uncertainty.

Accordingly, the comprehensive membership degree matrix B could then be determined by the evaluation matrix R and the index weight W by formula (5) for each grid, the final comprehensive risk distribution based on the maximum membership degree principle is displayed in Fig. 6(a), and the accordingly occupied area and percentages with different risk levels distributed by Re-classification tool in ArcGIS are shown in Fig. 6 (b) and (c):

The comparison of the comprehensive risk assessment distribution in Fig. 6(a) with the distribution of inundation depth in Fig. 4 denotes that most of the vulnerable submerged districts (in red color) with water depth over 0.5 m are contained within the high-risk level areas (painted in

Fig. 6 Comprehensive assessment of urban flooding risk in the study area: **a** the distribution of each risk level, **b** the occupied area of according risk level (hm^2), and **c** proportion of areas with corresponding risk level



pink in Fig. 6(a)), as these areas have adverse natural conditions and unfavorable drainage conditions. Although the high-risk level area only consists 5.06% of the total studied area in Fig. 6(c), the involved partition area with 42.13 hm² (shown in Fig. 6 (b)) also occupies large space, which calls for practical measures to prevent flooding events and to reduce losses with might and main. Besides, areas with medium- and high-risk levels (in Fig. 6(a)) are constantly in accordance with the agglomeration of residential area (in residential distribution map in Fig. 2(a)), because dense buildings and population may signify a great deal of hazard-bearing bodies. Moreover, the risk distributing pattern in Fig. 6(a) is quite similar with the distributional configuration of indexes of residential casualties, public psychology, and production efficiency (in Fig. 5 (d), (e), and (f)), and it is found that the less important AHP weight may not necessarily result in insignificant contribution to the comprehensive risk, as the AHP weight cannot directly determine the risk level. Indeed, the detailed GIS-based risk assessment method for each factor matters in the final comprehensive risk evaluation, which helps to quantify risks and reduce the subjective effect on AHP process for the final comprehensive risk assessment.

The application results confirm the applicability and effectiveness of the developed framework and platform in this study for the flooding risk assessment to provide optimal strategy and solution on resources allocation in detailed district for decision-makers under emergency rescue and disaster relief situations. According to the assessment results and findings of the studied district, under an extreme rainfall of 50-year recurrence interval, the percentage of different flooding risk levels (low, medium, or high risk) regions can be straightforwardly and intuitively identified as 56.31, 38.63, and 5.06%. Note that the high-risk regions with comprehensive assessment proportion accounted for relatively small proportion compared to the result with single-factor assessment, which implies the more dominated regional differences for comprehensive risk assessment. These distinct regions may denote the synthetic risk with low transport efficiency, high economic loss, high social impact on residential security, and high intangible damage, so the resilience strategy and measures would be more effectively accomplished, and the resources can be decently allocated to resist urban flooding in high-risk regions.

Conclusions

This paper proposed an integrated GIS-based flooding risk assessment framework for decision-makers under emergency rescue situations in central urban area of SA city. First, the distribution of inundation depth was simulated by the hydrology and hydraulic model of InfoWorks ICM,

so further flood-loss analysis could be conducted by 6 different depth-damage functions of flood-loss modes based on the calculated results. Specifically, these 6 methodically picked flooding assessment indicators could systematically evaluate different socioeconomic impacts and intangible flood loss for synthetic assessment, and the waterlogging loss map of each single factor assessment was presented by FCE method and GIS techniques, which can support better establishment of contingency plans with more efficient delivery of assistance and less flooding loss of both tangible and intangible damages. Finally, comprehensive risk assessment was accomplished by AHP method, and the high-risk level regions with low transport efficiency, high economic loss, high social impact, and high intangible damage only consisted 5.06% of the total studied area, where targeted improvement measures would be more effectively implemented. This investigated assessment framework can quantitatively analyze urban food risk with hydrology and hydraulic simulation and flood-loss functions, and is applicable to other cities with sufficient dataset for establishment and validation of hydrodynamic model and flood-loss model.

Further work could be extended to improve the risk assessment process by different aspects: 1) more hydraulic simulations with different rainstorm intensities, durations, or recurrence intervals could be tested to evaluate the influence of hazard factors; and 2) the scenarios of different flooding control methods such as advanced operation of pumping station or reconstruction of drainage pipelines in high-risk areas could be evaluated, and the comparison results may provide quantitative suggestion for decision-makers for better flooding management.

Author contribution All authors contributed to the study conception and design. Material preparation, data collection, and analysis were performed by Xiaolan Xiong, Hexiang Yan, Tao Tao, and Linsen Wang. The first draft of the manuscript was written by Fei Li and revised by Jie Ru Yan, and all authors commented on previous versions of the manuscript. All authors read and approved the final version of the manuscript.

Funding This research is financially supported by National Nature Science Foundation of China (Grant Nos. 52000142, 51978493 and 42001369) and Shanghai Pujiang Program (Grant No. 20PJ1417500).

Data availability All data generated or analyzed during this study are included in this published article.

Declarations

Ethics approval This research did not contain any studies involving animal or human participants, nor did it take place on any private or protected areas. No specific permissions were required for corresponding locations.

Competing interests The authors declare no competing interests.

References

- Boyd E, Levitan M, Van Heerden I (2005) Further specification of the of the dose-response relationship for flood fatality estimation. The US-Bangladesh Workshop on Innovation in Wind-storm/storm Surge Mitigation Construction, Dhaka
- Brussee AR, Bricker JD, De Bruijn KM, Verhoeven GF, Winsemius HC, Jonkman SN (2021) Impact of hydraulic model resolution and loss of life model modification on flood fatality risk estimation: case study of the Bommelerwaard The Netherlands. *J Flood Risk Manag* 14(3):15. <https://doi.org/10.1111/jfr3.12713>
- Cai T, Li XY, Ding X, Wang J, Zhan J (2019) Flood risk assessment based on hydrodynamic model and fuzzy comprehensive evaluation with GIS technique. *Int. J. Disaster Risk Reduct* 35:101077. <https://doi.org/10.1016/j.ijdr.2019.101077>
- Dassanayake DR, Burzel A, Oumeraci H (2015) Methods for the evaluation of intangible flood losses and their integration in flood risk analysis. *Coast Eng J* 57(1):35. <https://doi.org/10.1142/s0578563415400070>
- Dutta D, Herath S, Musiakac K (2003) A mathematical model for flood loss estimation. *J Hydrol* 277(1–2):24–49. [https://doi.org/10.1016/S0022-1694\(03\)00084-2](https://doi.org/10.1016/S0022-1694(03)00084-2)
- Geng YF, Zheng X, Wang ZL, Wang ZW (2020) Flood risk assessment in Quzhou City (China) using a coupled hydrodynamic model and fuzzy comprehensive evaluation (FCE). *Nat Hazards* 100(1):133–149. <https://doi.org/10.1007/s11069-019-03803-0>
- Ger IT, Kreibich H, Franco G, Marechal D, Schroter K (2016) A review of flood loss models as basis for harmonization and benchmarking. *PLoS ONE* 11(7):22. <https://doi.org/10.1371/journal.pone.0159791>
- Gigovic L, Pamucar D, Bajic Z, Drobnjak S (2017) Application of GIS-interval rough AHP methodology for flood hazard mapping in urban areas. *Water* 9(6). <https://doi.org/10.3390/w9060360>
- Gong YW, Li XN, Zhai DD, Yin DK, Song RN, Li JQ, Yuan DH (2018) Influence of rainfall, model parameters and routing methods on stormwater modelling. *Water Resour Manag* 32(2):735–750. <https://doi.org/10.1007/s11269-017-1836-x>
- Hammond MJ, Chen AS, Djordjevic S, Butler D, Mark O (2015) Urban flood impact assessment: a state-of-the-art review. *Urban Water J* 12(1):14–29. <https://doi.org/10.1080/1573062x.2013.857421>
- Handmer JW, Reed C, Percovich O (2002) Disaster loss assessment: guidelines. Department of Emergency Services and Centre for Risk and Community Safety [Brisbane]. <http://nla.gov.au/nla.arc-58965>
- Herath S, Dutta D, Musiakac K (2003) A mathematical model for flood loss estimation. *J Hydrol* 277(1–2):24–49. [https://doi.org/10.1016/S0022-1694\(03\)00084-2](https://doi.org/10.1016/S0022-1694(03)00084-2)
- Hudson P, BotzenWJW PJ, Aerts J (2019) Impacts of flooding and flood preparedness on subjective well-being: a monetisation of the tangible and intangible impacts. *J Happiness Stud* 20(2):665–682. <https://doi.org/10.1007/s10902-017-9916-4>
- Intergovernmental Panel on Climate Change (IPCC) (2022) Climate change 2022: impacts, adaptation and vulnerability. Available online: <https://www.ipcc.ch/report/ar6/wg2/>. Accessed 28 Feb 2022
- Jonkman SN (2005) Global perspectives on loss of human life caused by floods. *Nat Hazards* 34(2):151–175. <https://doi.org/10.1007/s11069-004-8891-3>
- Kia MB, Pirasteh S, Pradhan B, Mahmud AR, Sulaiman WNA, Moradi A (2012) An artificial neural network model for flood simulation using GIS: Johor River Basin, Malaysia. *Environ Earth Sci* 67(1):251–264. <https://doi.org/10.1007/s12665-011-1504-z>
- Lai CG, Chen XH, Chen XY, Wang ZL, Wu XS, Zhao SW (2015) A fuzzy comprehensive evaluation model for flood risk based on the combination weight of game theory. *Nat Hazards* 77(2):1243–1259. <https://doi.org/10.1007/s11069-015-1645-6>
- Lekuthai A, Vongvisessomjai S (2001) Intangible flood damage quantification. *Water Resour Manag* 15(5):343–362. <https://doi.org/10.1023/A:1014489329348>
- Li F, Duan HF, Yan HX, Tao T (2015) Multi-objective optimal design of detention tanks in the urban stormwater drainage system: framework development and case study. *Water Resour Manag* 29(7):2125–2137. <https://doi.org/10.1007/s11269-015-0931-0>
- Lv H, Guan XJ, Meng Y (2020) Comprehensive evaluation of urban flood-bearing risks based on combined compound fuzzy matter-element and entropy weight model. *Nat Hazards* 103(2):1823–1841. <https://doi.org/10.1007/s11069-020-04056-y>
- Lyu HM, Zhou WH, Shen SL, Zhou AN (2020) Inundation risk assessment of metro system using AHP and TFN-AHP in Shenzhen. *Sustain Cities Soc* 56:14. <https://doi.org/10.1016/j.cs.2020.102103>
- Marvi MT (2020) A review of flood damage analysis for a building structure and contents. *Nat Hazards* 102(3):967–995. <https://doi.org/10.1007/s11069-020-03941-w>
- Nithila AN, Shome P, Islam I (2022) Waterlogging induced loss and damage assessment of urban households in the monsoon period: a case study of Dhaka, Bangladesh. *Nat Hazards* 110(3):1565–1597. <https://doi.org/10.1007/s11069-021-05003-1>
- Oubennaceur K, Chokmani K, Nastev M, Lhissou R, El Alem A (2019) Flood risk mapping for direct damage to residential buildings in Quebec, Canada. *Int J Disaster Risk Reduct* 33:44–54. <https://doi.org/10.1016/j.ijdr.2018.09.007>
- Quan RS (2014a) Vulnerability analysis of rainstorm flooding on buildings in central urban area of Shanghai based on scenario simulation. *Sci Geogr Sin* 34(11):1399–1403 in Chinese
- Quan RS (2014b) Rainstorm waterlogging risk assessment in central urban area of Shanghai based on multiple scenario simulation. *Nat Hazards* 73(3):1569–1585. <https://doi.org/10.1007/s11069-014-1156-x>
- SDOWE (Standard for Design of Outdoor Wastewater Engineering) (2021) The People's Republic of China Ministry of Housing and Urban Rural Development pp. 11–14
- Tehrany MS, Pradhan B, Jebur MN (2013) Spatial prediction of flood susceptible areas using rule-based decision tree (DT) and a novel ensemble bivariate and multivariate statistical models in GIS. *J Hydrol* 504:69–79. <https://doi.org/10.1016/j.jhydrol.2013.09.034>
- Teng J, Jakeman AJ, Vaze J, Croke BFW, Dutta D, Kim S (2017) Flood inundation modelling: a review of methods, recent advances and uncertainty analysis. *Environ Model Softw* 90:201–216. <https://doi.org/10.1016/j.envsoft.2017.01.006>
- The Global Risks Report (2022) 17th Edition (2022) The world economic forum, ISBN: 978–2–940631–09–4
- Wallingford (1981) Design and analysis of urban stormwater drainage—the Wallingford procedure. Department of Environment, National Water Council, UK
- Wallingford (2015) InforWorks ICM product information-overview. Available online: http://www.innovyze.com/products/infoworks_icm
- Wang P (1983) Fuzzy sets and their application. Shanghai Science and Technology Press, Shanghai
- Wang HY (2002) Assessment and prediction of overall environmental quality of Zhuzhou City, Hunan Province, China. *J Environ Manage* 66(3):329–340. <https://doi.org/10.1006/jema.2002.0590>
- Wang Y, Li Z, Tang Z, Zeng G (2011) A GIS-based spatial multi-criteria approach for flood risk assessment in the Dongting Lake Region, Hunan Central China. *Water Resour Manag* 25(13):3465–3484. <https://doi.org/10.1007/s11269-011-9866-2>
- Wang H, Zhou JJ, Tang Y, Liu ZL, Kang AQ, Chen B (2021) Flood economic assessment of structural measure based on integrated flood risk management: a case study in Beijing. *J Environ Manage* 280:9. <https://doi.org/10.1016/j.jenvman.2020.111701>

- Win S, Zin WW, Kawasaki A, San Z (2018) Establishment of flood damage function models: a case study in the Bago River Basin, Myanmar. *Int J Disaster Risk Reduct* 28:688–700. <https://doi.org/10.1016/j.ijdrr.2018.01.030>
- Xinhua News Agency (2022) An investigation report on “Zhengzhou 7.20 Storm” in Henan province. Available online: http://www.gov.cn/xinwen/2022-01/21/content_5669723.htm. Accessed 21 Jan 2022
- Xue XH, Yang XG (2014) Seismic liquefaction potential assessed by fuzzy comprehensive evaluation method. *Nat Hazards* 71(3):2101–2112. <https://doi.org/10.1007/s11069-013-0997-z>
- Yager RR (1977) Multiple objective decision-making using fuzzy sets. *Int J Man Mach Stud* 9(4):375–382. [https://doi.org/10.1016/S0020-7373\(77\)80008-4](https://doi.org/10.1016/S0020-7373(77)80008-4)
- Zabret K, Hozjan U, Kryzanowsky A, Brilly M, VidmarA, (2018) Development of model for the estimation of direct flood damage including the movable property. *J Flood Risk Manag* 11:S527–S540. <https://doi.org/10.1111/jfr3.12255>
- Zhao J (2015) Urban flooding impact on traffic attenuation model. Dissertation, Beijing University of Technology:Beijing
- Zheng Q, Shen SL, Zhou AN, Lyu HM (2022) Inundation risk assessment based on G-DEMATEL-AHP and its application to Zhengzhou flooding disaster. *Sustain Cities Soc* 86:. <https://doi.org/10.1016/j.scs.2022.104138>

Publisher's note Springer Nature remains neutral with regard to jurisdictional claims in published maps and institutional affiliations.

Springer Nature or its licensor (e.g. a society or other partner) holds exclusive rights to this article under a publishing agreement with the author(s) or other rightsholder(s); author self-archiving of the accepted manuscript version of this article is solely governed by the terms of such publishing agreement and applicable law.